Analysis of Short-Circuit Performance of Split-Winding Transformer Using Coupled Field-Circuit Approach

G. B. Kumbhar and S. V. Kulkarni, *Member, IEEE*

***Abstract*—The split-winding arrangement requires special short-circuit design considerations. During short-circuit conditions, there is a considerable distortion of the leakage field, which in turn produces high axial short-circuit forces. This paper deals with the computation and analysis of electromagnetic forces in windings of split-winding transformers. A nonlinear-transient field-circuit coupled finite element model is used to simulate the split-winding transformer. A 70-MVA, three-phase, 220/6.9/6.9-kV split-winding transformer is modeled under preset and postset short-circuit test conditions. Under the preset condition, the transformer is analyzed with one as well as both the LV windings short circuited to compare the axial forces produced in the windings for these two cases. The results show that there is a considerable rise in the axial forces when one winding is short circuited as compared with the case when both windings are short circuited. The effect of initial magnetization of core on axial short-circuit forces is calculated and discussed. It is also shown that even though postset method eliminates inrush related problems there is not much respite in short-circuit forces.**

***Index Terms*—Field-circuit coupling, finite-element method (FEM), nonlinear transient, split-winding transformer.**

I. Introduction

THE transformer is a very critical and costly equipment in power systems. The addition of more generating capacities and interconnections in power systems has contributed to an increase in short-circuit capacity of networks, making the short-circuit duty of transformers more severe. Failure of transformers due to short circuits is a major concern for power utilities and manufacturers. An inadequate short-circuit strength may lead to a mechanical collapse of windings and deformation or damage to the clamping structure. The short-circuit design is one of the most important and challenging aspects of transformer design. Designers need advanced analysis tools that can simulate short-circuit performance of transformers. These days, owing to a quantum improvement in computational facilities, transient analysis of complex electromagnetic devices has become feasible, which can help in performing simulation studies for an in-depth analysis of various phenomena affecting their reliability. In recent times, field-circuit-coupled formulation has become an important tool in design, analysis and nondestructive testing of electromagnetic devices. The field part is generally solved by using the well-known finite-element method (FEM) while the circuit part is solved using nodal or loop circuit analysis [1]–[3].

In the past, classical methods were used to compute the short-circuit forces in windings. These methods use simplified configurations and make assumptions such as infinite permeability of core material [4]. Although these methods are simple, fast and easy to formulate, they are not suitable for predicting the performance of special types of transformers. Over the years, many accurate electromagnetic force computation methods have been proposed in the literature mainly based on static formulations [5]–[9]. Transient formulations are described in [10]–[12]. Analysis of split-winding transformers requires a field-circuit approach with magnetic nonlinearity taken into account.

The split-winding arrangement is particularly used in power transformers. It usually consists of several pairs of input and output windings. All the input windings are connected in parallel and all the output windings are independent and galvanically separated from each other. The functions of the input and output windings can be interchanged. One typical configuration is shown in Fig. 1. Two secondary windings are placed axially with respect to each other (LV1 and LV2). The primary windings are also split into two parts with center-line lead arrangement (HV1 and HV2). Advantages of the transformer with split-winding arrangement include saving of space/instrumentation and decrease in values of short-circuit currents in the individual circuits [13], [14]. However, split-winding transformers require special short-circuit design considerations since there is a considerable distortion of the leakage field under specific conditions, which in turn produces high axial short-circuit forces and end thrusts in the windings under short circuit [15].

Very few published papers have reported the analysis of short-circuit performance of the split-winding transformers. Previously, this phenomenon was analyzed using a magnetic equivalent circuit model (MEC) or reluctance network model [14]. Although, such a model is simple and gives a fast solution, it contains some peculiarities. First, the number of elements employed are small and this may reduce accuracy of the solution. Moreover, it is difficult to calculate the field quantities at any specified locations. The second peculiarity is that the flux flowing through a reluctance element is assumed to pass through a specified direction only. On the other hand, FEM is very flexible and the directions of flux paths need not be known in advance. As far as split-winding transformers are concerned,

Manuscript received December 22, 2005; revised July 28, 2006. This work was supported by the Department of Science and Technology, Government of India, under Project SR/FTP/ET-165/2001. Paper no. TPWRD-00734-2005.

The authors are with the Department of Electrical Engineering, Indian Institute of Technology–Bombay, Mumbai 400076, India (e-mail: ganeshk@iitb.ac.in; svk@ee.iitb.ac.in).

Color versions of one or more of the figures in this paper are available online at http://ieeexplore.ieee.org.

Digital Object Identifier 10.1109/TPWRD.2007.893442

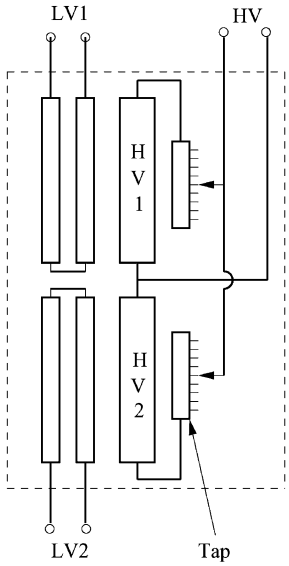

Fig. 1. Arrangement and electrical winding connections of the split-winding transformer.

short-circuit test on only one LV winding leads to considerable distortion of leakage field and this distortion may not be captured accurately using the MEC method. With the use of field-circuit coupled FEM model, currents in various parts of the model are not required to be known in advance; induced currents are automatically calculated. Furthermore, the flux flowing through the limbs, on which the windings are placed, is decided by the voltages applied to the windings.

In this work, a comprehensive analysis of a split-winding transformer is done to assess its short-circuit performance under preset and postset short-circuit test conditions. The axial and radial forces are computed using nonlinear-transient field-circuit coupled formulation. Nonlinearity is taken into account by using the actual B–H curve of the core material. This paper describes in detail the formulation, modeling and analysis of the split-winding transformer. A 2-D axisymmetric model is developed based on the method described in [16]. First, the validity of this model is verified by using complete 3-D model. The distribution of radial and axial forces on the windings are computed under the preset (considering various initial magnetization conditions) and postset short-circuit conditions using the developed 2-D axisymmetric model. In the preset short-circuit condition, the transformer is analyzed with one as well as both the LV windings short circuited to compare the axial forces produced in the windings for these two cases.

II. Coupled Field-Circuit Formulation

A. Electromagnetic Model

For 2-D axisymmetric magnetic analysis, consider the classical Poisson's equation [17]

$$\frac{\partial}{\partial r}\left(\frac{1}{r}\frac{1}{\mu}\frac{\partial A_R}{\partial r}\right)+\frac{\partial}{\partial z}\left(\frac{1}{r}\frac{1}{\mu}\frac{\partial A_R}{\partial z}\right)=-J_\phi \tag{1}$$

where $A_R(=rA_\phi)$ and J_ϕ denote the magnetic vector potential and the free or the source current density respectively, and μ is the material permeability.

It is assumed that the windings are made up of thin stranded conductors. These thin stranded conductors can be modeled as carrying uniform current densities (i.e., the induction term in the magnetic-field equations representing eddy currents is neglected). Assuming that each turn carries I amperes of current, the magnitude of current density in a winding is

$$J_\phi = d\frac{nI}{S_c} \tag{2}$$

where n and S_c are the number of turns and the cross-sectional area of the winding respectively, and d is the polarity ($+1$ or -1) to represent the forward or the return path in ϕ-direction. After space discretization of (1) using Galerkin method [18], we have

$$[K]\{A_R\}+[D]\{I\}=0 \tag{3}$$

where

$$[K]=\sum_\Omega \frac{1}{r}\frac{1}{\mu}\iint_{\Delta_e}\left(\frac{\partial N_e^T}{\partial r}\frac{\partial N_e}{\partial r}+\frac{\partial N_e^T}{\partial z}\frac{\partial N_e}{\partial z}\right)drdz$$

$$[D]=\sum_\Omega \frac{n}{S_c}\iint_{\Delta_e} N_e^T drdz$$

where N_e and Δ_e are the element shape function and the element area, respectively, and Ω indicates the domain under consideration.

B. External Circuit Equations

The matrix form of the external circuit equations can be written as

$$[U]=\left\{\frac{d\Phi}{dt}\right\}+[R]\{I\}+[L]\left\{\frac{dI}{dt}\right\}. \tag{4}$$

If flux linkages are expressed in terms of the magnetic vector potential, the matrix form of the external circuit equations can be written as

$$[U]=[G]\left\{\frac{dA_R}{dt}\right\}+[R]\{I\}+[L]\left\{\frac{dI}{dt}\right\} \tag{5}$$

where U is the vector of input voltages, $[L]$ and $[R]$ are the matrices of leakage inductances and winding resistances, respectively, and G is a matrix similar to D and it depends on the geometrical features of the windings.

C. Nonlinear-Transient Field-Circuit Coupled Model

From (3) and (5), the field-circuit coupled global system of equations can be written as

$$\begin{bmatrix}0 & 0\\ G & L\end{bmatrix}\begin{Bmatrix}\dot{A_R}\\ \dot{I}\end{Bmatrix}+\begin{bmatrix}K & D\\ 0 & R\end{bmatrix}\begin{Bmatrix}A_R\\ I\end{Bmatrix}=\begin{Bmatrix}0\\ U\end{Bmatrix}. \tag{6}$$

In this system of equations, the unknowns are the nodal values of the vector potential (A_R) and the currents in the external circuits (I). To solve this time dependent system of equations, a numerical integration scheme such as Euler

Backward or Crank–Nicholson algorithm can be used. The nonlinearities in the modeled system are taken into account by using Newton–Raphson iterative procedure. The resulting system of equations is

$$\begin{aligned}&\begin{bmatrix}\beta\left(K^n+K_{nl}^n\right) & \beta D\\ \frac{G}{\Delta t} & \beta R+\frac{L}{\Delta t}\end{bmatrix}\begin{Bmatrix}\Delta A_R\\ \Delta I\end{Bmatrix}_{t+\Delta t}^{n+1}\\ &\quad=\begin{Bmatrix}0\\ \beta V_{t+\Delta t}+(1-\beta)V_t\end{Bmatrix}\\ &\quad+\begin{bmatrix}-(1-\beta)K & -(1-\beta)D\\ \frac{G}{\Delta t} & -(1-\beta)R+\frac{L}{\Delta t}\end{bmatrix}\begin{Bmatrix}A_R\\ I\end{Bmatrix}_t\\ &\quad-\begin{bmatrix}\beta(K^n) & \beta D\\ \frac{G}{\Delta t} & \beta R+\frac{L}{\Delta t}\end{bmatrix}\begin{Bmatrix}A_R\\ I\end{Bmatrix}_{t+\Delta t}^{n}\end{aligned}\tag{7}$$

where the term K_{nl}^n accounts for the nonlinearity of the core material. The value of β determines the nature of the time-stepping scheme [18].

III. Simulation Methodology

A 70-MVA, three-phase, 220/6.9/6.9-kV split-winding transformer has been analyzed under various short-circuit test conditions. The transformer is analyzed on per-phase basis which is generally done. The forces acting on the middle phase have been calculated for the front view (parallel to the core plane) and end view (normal to the core plane). Design details and nameplate data of the considered transformer are given in the Appendix. Fig. 1 shows the arrangement of the split-winding transformer. Although, within the core window the Cartesian 2-D formulations are sufficiently accurate, a 3-D method should be used for accurate estimation of forces outside it since there may be appreciable variation of forces along the winding circumference. However in the 3-D case, to calculate force distribution accurately, large number of elements is required. Thus, to model the transformer using transient-nonlinear FE formulation with large number of unknowns, the computational efforts increase manifold. On the other hand, the model suggested in [16] uses 2-D axisymmetric analysis to yield the field quantities with a reasonable accuracy. Fig. 2 shows the equivalent 2-D simplified axisymmetric model with specially shaped yokes and outer limbs to get same cross-sectional area as well as same reluctance. The validity of this model is verified by comparing the values of forces with complete nonlinear 3-D model. The results obtained using the classical method [4], [15], the 3-D method and the simplified 2-D axisymmetric method (front and end view) are given in Table I (with one winding short circuited). The classical values are calculated by using the short-circuit currents obtained from 3-D FEM analysis. The 2-D simulations for end view are done using large size core window. From Table I, it can be seen that the force values calculated using the 3-D and the simplified 2-D axisymmetric (front and end views) methods agree fairly with each other. However, the solution using the 2-D method is obtained much faster and the computational efforts required are much less. Forces on the outer limb windings can be considered approximately equal to the values obtained in the end view using the equivalent 2-D simplified analysis. It can be seen from Table I that the total winding forces in the front and end views are quite close, although the local values of the forces may differ slightly.

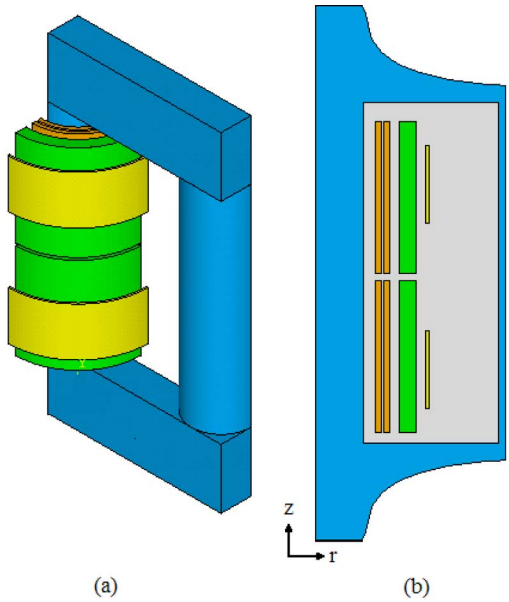

Fig. 2. (a) The 3-D model and (b) equivalent 2-D simplified geometry.

TABLE I
Comparison of Results

		Radial forces in Tons		
		LV2 (inner)	LV2 (outer)	HV2
Classical		173.92	521.77	954.48
Nonlinear 3-D		145.45	556.96	801.79
2-D simplified geometry	Front view	136.50	520.41	804.91
	End view	133.61	538.76	808.33

Nonlinear transient field-circuit-coupled finite-element analysis is carried out using code developed in MATLAB based on the methodology given in Section II. The windings are modeled with stranded conductors. The results from the developed code have been verified using a commercial FEM software. The nonlinearity of the core material is taken into account by using the B–H curve of the M3H material (see the Appendix).

The flux density distribution obtained can be used to calculate the forces experienced by the windings. The local force density $\mathbf{F}$ in the winding is computed from the vector product of current density $\mathbf{J}$ and local magnetic flux density $\mathbf{B}$

$$\mathbf{F}=\mathbf{J}\times\mathbf{B}.\tag{8}$$

To compute the distribution of forces, each winding is divided into 20 subregions along the height. The axial and radial components of the force densities are computed by using the corresponding components of the flux densities and the current densities of elements ($F_{\text{rad}}=B_z\times J_\phi$ and $F_{\text{axi}}=B_r\times J_\phi$). The total axial and radial forces on each subregion are computed by integrating the element force densities.

IV. Results and Discussion

A. Preset Method

First, the transformer is simulated under the preset short-circuit test condition, which is the generally used short-circuit test

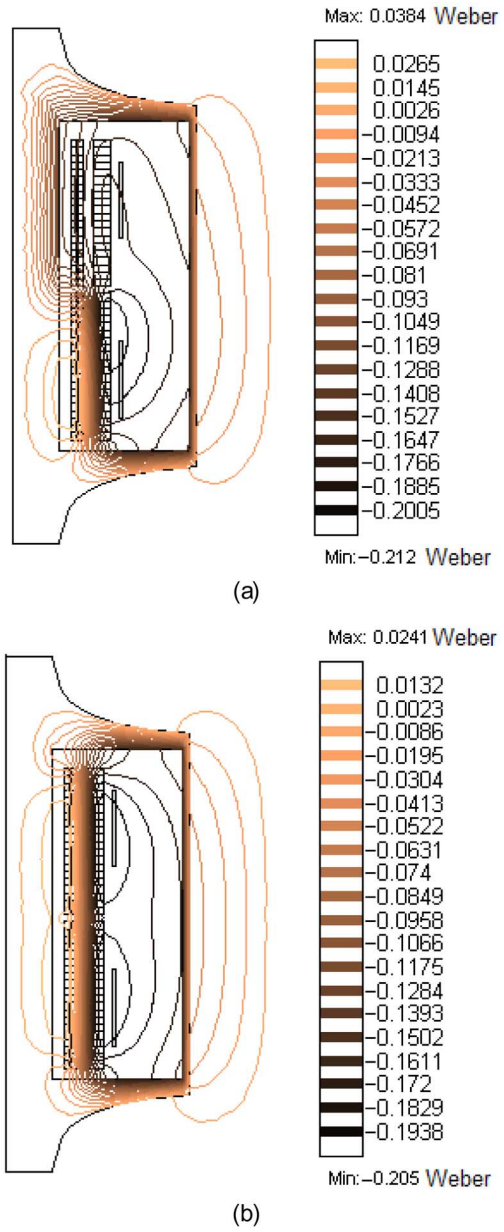

Fig. 3. Contour lines of magnetic vector potential for the cases when (a) one winding is short circuited and (b) both windings are short circuited.

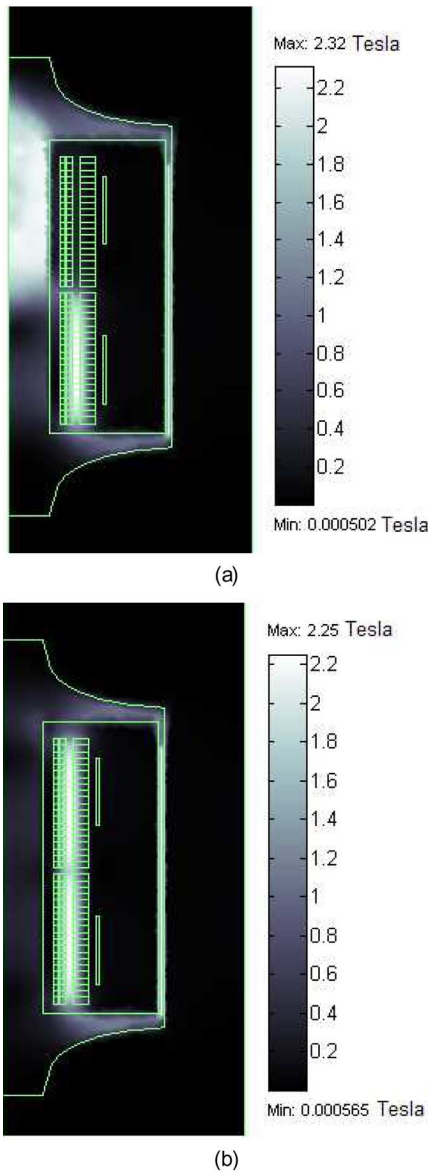

Fig. 4. Flux density plots when (a) one winding is short circuited and (b) both windings are short circuited.

method (the postset method is not used because of test plant limitations) [14]. In this method, the LV winding is short circuited before closing the circuit breaker at the source terminals. The HV windings are connected in parallel and supplied from a voltage source.

Two cases are analyzed in the preset test condition. In the first case, one LV winding (LV2) is short circuited using a low value resistance, while the other is open circuited using a high value resistance. In the second case, both the LV windings are short circuited. The initial magnetization of core is assumed to be zero during the simulation. The radial and the axial forces are computed at the first peak of the short-circuit current.

In the single short-circuited winding case, the flux distribution is completely different in the lower and upper parts of the core limb. Fig. 3(a) and (b) shows the flux patterns, and Fig. 4(a) and (b) shows plots of the flux densities for the two considered cases at the first peak of the short-circuit current. The flux density in the upper part of the limb is very high (about 2.2 T) with a corresponding high inrush current for the HV1 winding [see Fig. 5(a)], whereas there is no demand for significant magnetizing current by the HV2 winding since the flux density in the bottom part of the limb is very low due to the short-circuited inner LV2 winding. The upper half of the limb becomes saturated while the lower part is well below saturation. This phenomenon results in heavy distortion of fields in the core and the windings, and leads to higher axial short-circuit forces in LV2 and HV2. Fig. 5(b) shows the waveform of the short-circuit current in the HV2 winding. The values of winding currents are given in Table II (per unit values are based on 35 MVA). The inrush current flows mainly in the HV1 winding due to the reason explained previously. The simulation results give the terminal

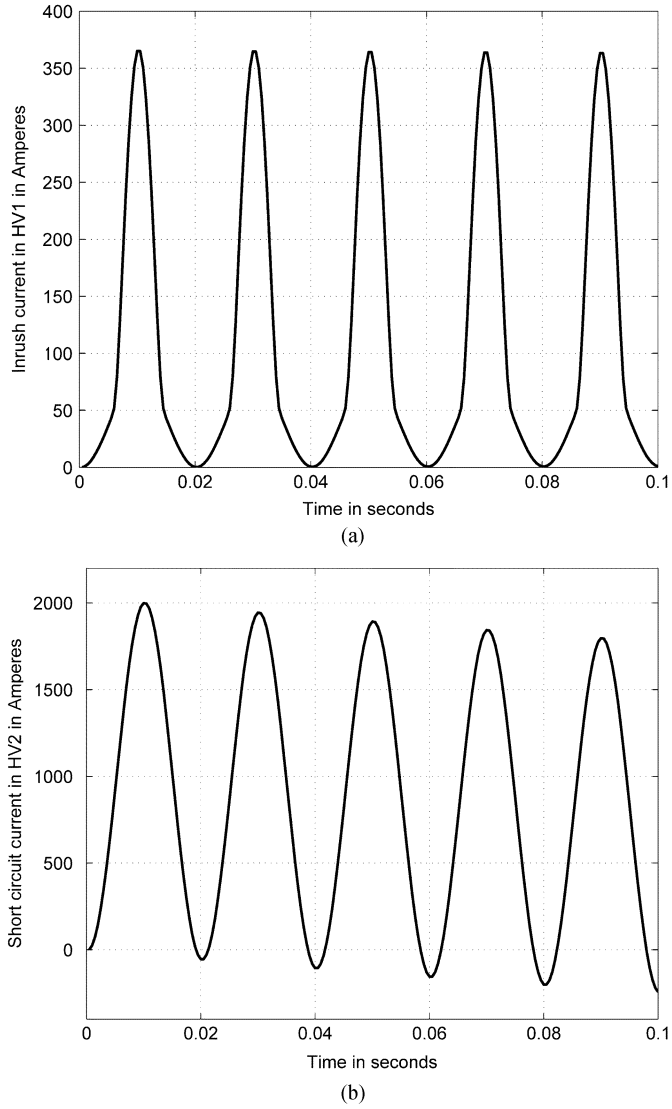

Fig. 5. (a) Inrush current in HV1 and (b) short-circuit current in HV2.

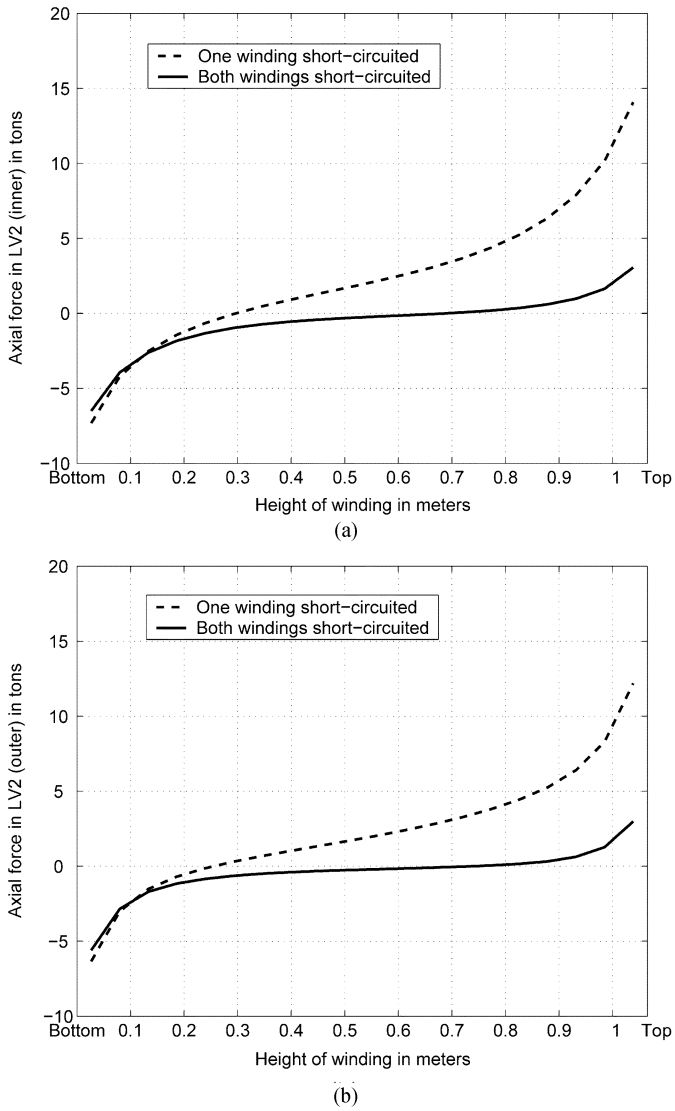

Fig. 6. Axial forces in LV2 winding (a) inner and (b) outer.

TABLE II
MAXIMUM PEAK WINDING CURRENTS DURING PRESET METHOD

windings	Currents in Amperes
HV1	365 (3.97 p.u.)
HV2	1998 (21.75 p.u.)
LV2	65292 (22.29 p.u.)

HV current (phasor addition of currents in HV1 and HV2) to be about 18% higher than the HV2 current.

Fig. 6(a) and (b) shows the axial forces along the height of the winding for the inner and outer LV2 windings, respectively. The radial force distribution is given in Fig. 7(a) and (b) for the inner and outer LV2 windings, respectively. The results are shown for both the considered cases. It is seen that for the same value of short-circuit current, the axial forces are higher for the case in which only one of the LV windings is short circuited as compared to the case when both the LV windings are short circuited. There is no appreciable change in the radial forces since the inrush current flows mainly in HV1. Fig. 8(a) and (b) shows the axial and radial forces along the height of the HV2 winding, respectively.

The total radial forces for the considered windings are summarized in Table III. For the other windings the forces are not appreciable. It is seen that there is moderate change in the radial force in the windings because of corresponding small change in the axial component of flux densities. The negative sign indicates negative r and z directions for the radial and axial forces, respectively. Table IV gives the axial forces on the windings. It is seen that the values of net axial forces are much larger in the case when one winding is short circuited. In the case of HV2, even though it is not explicit from the force distribution plot, there is a considerable amount of net force acting on it. It is also noted that the net axial force acting on the HV2 winding is in opposite direction to that acting on the LV2 winding. If the clamping structures are not designed properly to account for these net forces, axial displacements of windings may occur.

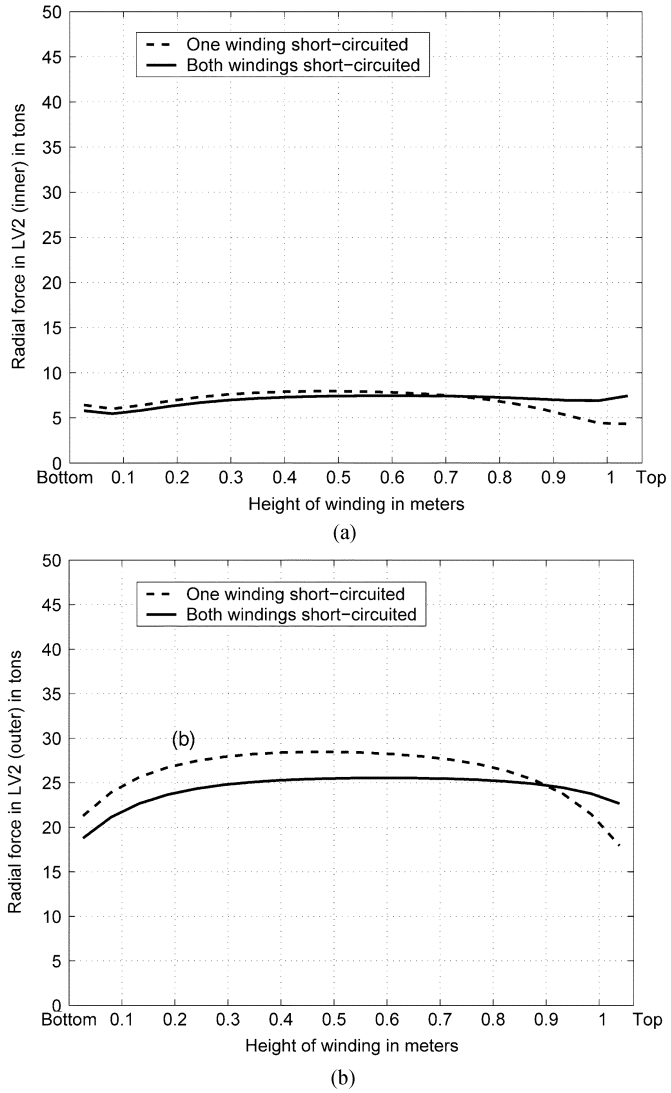

Fig. 7. Radial forces in LV2 winding (a) inner and (b) outer.

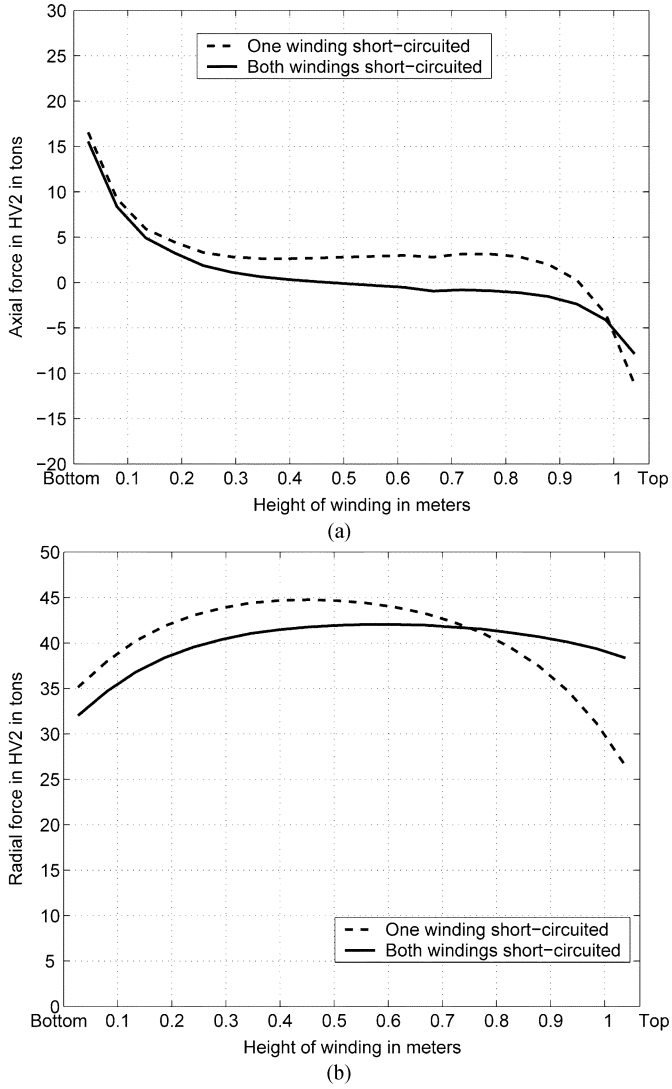

Fig. 8. (a) Axial forces. (b) Radial forces in the HV2 winding.

B. *Effect of Initial Magnetization*

Often the core retains residual magnetism due to earlier short-circuit tests. The magnitude and polarity of the residual flux in the transformer core at the instant of energization affects the inrush current in the HV1 winding resulting into redistribution of forces. Typical magnitudes of residual core flux are in the range of 20% to 80% of peak normal flux. In this study, three cases of initial magnetization are considered with residual flux densities, viz., -0.8 T, 0 T, and $+0.8$ T. The residual magnetism is taken into account by adding the corresponding magnetization term in the formulation to provide dc bias. The values of HV1 winding currents for different magnetization conditions are listed in Table V. It can be seen that the value of inrush current increases with an increase in value of residual flux density. Table VI gives the values of axial forces for different magnetization conditions. The trends in the forces agree closely with those given in [14]. The results also emphasize the fact that the forces reduce if the core is deliberately pre-magnetized with opposite polarity. The results for the postset method (to be discussed in the following subsection) are also given for ready comparison.

TABLE III
TOTAL RADIAL FORCES IN TONS

Winding	Both windings Short-circuited	One winding Short-circuited
LV2 (inner)	-138.88	-136.50
LV2 (outer)	-484.86	-520.41
HV2	796.787	804.91

TABLE IV
TOTAL AXIAL COMPRESSIVE FORCES IN TONS

Winding	Both windings short-circuited			One winding short-circuited		
	down-ward	up-ward	net	down-ward	up-ward	net
LV2 (inner)	-6.84	19.61	12.76	-63.92	16.17	-47.73
LV2 (outer)	-5.40	14.71	9.31	-55.91	11.70	-44.21
HV2	-20.73	41.2	20.46	83.39	-14.69	68.70

TABLE V
COMPARISON OF MAXIMUM PEAK WINDING CURRENTS FOR VARIOUS MAGNETIZATION CONDITIONS

Winding	Preset method			Post-set method
	-0.8 T	0 T	+0.8 T	
HV1 current (Amps)	139.4	365	654.2	88.6
HV2 current (Amps)	1978.6	1998.1	2019.0	1885.5

TABLE VI
COMPARISON OF AXIAL FORCES FOR VARIOUS MAGNETIZATION CONDITIONS

Winding	Preset method			Post-set method
	-0.8 T	0 T	+0.8 T	
LV2 (inner)	46.03	47.73	40.85	43.22
LV2 (outer)	41.80	44.21	38.93	39.00
HV2	57.30	68.21	68.69	50.88

TABLE VII
MAXIMUM PEAK WINDING CURRENTS DURING POSTSET METHOD

windings	Currents in Amperes
HV1	88.6 (0.965 p.u.)
HV2	1855 (20.19 p.u.)
LV2	61327 (20.93 p.u.)

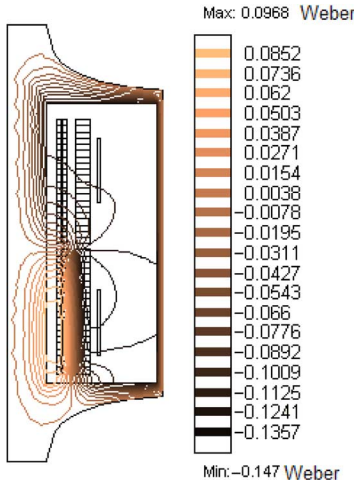

Fig. 9. Contour lines of magnetic vector potential for postset method.

TABLE VIII
TOTAL FORCES IN TONS DURING POSTSET METHOD

Winding	Radial Forces in tons	Axial forces in tons		
		downward	upward	net
LV2 (inner)	-132.07	-59.69	16.47	-43.22
LV2 (outer)	-505.29	-50.99	12.00	-39.00
HV2	785.96	68.96	-18.08	50.88

C. Postset Method

If the short-circuit capacity of the station is high enough to allow the postset method (which eliminates the inrush and related problems), there is still one more characteristic of the split-winding transformer which makes the short-circuit test on them more severe than the conventional two winding transformers. With the LV2 winding short circuited, some current flows in the HV1 winding which is not directly facing the short-circuited LV2 winding. The transformer when simulated for the postset short-circuit condition, LV2 is short circuited after decay of inrush currents in the HV1 and HV2 windings. Table VII gives the values of short-circuit currents in the windings during the postset method. The calculated value of current in HV1 is 4.78% of the short-circuit current flowing in HV2. It is generally small, in the range of 3% to 5% of that flowing in the HV2 winding due to a much higher impedance between the HV1 and LV2 windings, but it is sufficient to cause ampere-turn unbalance along the height of the windings. The ampere-turns of HV2 are smaller than that of LV2, and corresponding to the ampere-turns of HV1 there are no balancing ampere-turns in LV1 (since it is open circuited). Hence, there is considerable distortion of the leakage field (see Fig. 9) resulting into higher axial short-circuit forces. Table VIII gives the values of forces during the postset short-circuit method. Even though the postset method eliminates the inrush related problems, there is not much respite in the short-circuit stresses (as compared to the case of both the windings short circuited).

It can be also noted that the effect of short-circuit current share between HV1 and HV2 (approximately 5% and 95%) is also present in the preset method. Thus, the current shown in Fig. 5(a) is actually a superposition of inrush current and the HV1 share. Currents such as this HV1 current or inrush currents (in the HV1 and HV2 windings) create asymmetry in the maximum positive and negative potential values in the magnetic vector potential plot.

Thus, although the split-winding configuration helps in limiting the rating of circuit breakers, it poses problems for the short circuit withstand. The high axial short-circuit forces could lead to deformation in the end clamping structure and the windings as well. The end clamping structure plays an important role in resisting axial forces during short circuit. This puts emphasis on accurate evaluation of these axial forces.

V. CONCLUSION

This paper has presented a detailed formulation and modeling to evaluate the short-circuit performance of the split-winding transformers. A 70-MVA, three-phase, 220/6.9/6.9-kV split-winding transformer is modeled under short-circuit test conditions. A 2-D axisymmetric field-circuit-coupled nonlinear transient finite-element model has been developed to investigate transient axial and radial forces in the windings. The results of the model have been verified with the 3-D model. Simulation results are reported for both preset (with various initial magnetization conditions) and postset short-circuit test conditions.

Under the preset short-circuit condition, the axial and radial forces are computed for two cases, viz. only one winding short circuited and both windings short circuited. In the former case, there is considerable distortion of leakage field resulting in higher axial short-circuit forces. For the same value of short-circuit current, the forces are higher for this case as compared to the latter case in which both the windings are short circuited. Also, the beneficial effect of deliberate pre-magnetization with opposite polarity is demonstrated.

TABLE IX
TRANSFORMER DATA

Rated HV1 and HV2 currents	91.85 Amps
Rated LV1 and LV2 currents	2928.6 Amps
Number of HV1 and HV2 turns	1039
Number of Tap turns at normal tap	13
Number of LV1 and LV2 turns	33
Percentage impedance	13.9
Tap setting	Normal
Core area	3236.6 cm^2
Core steel type	M3H

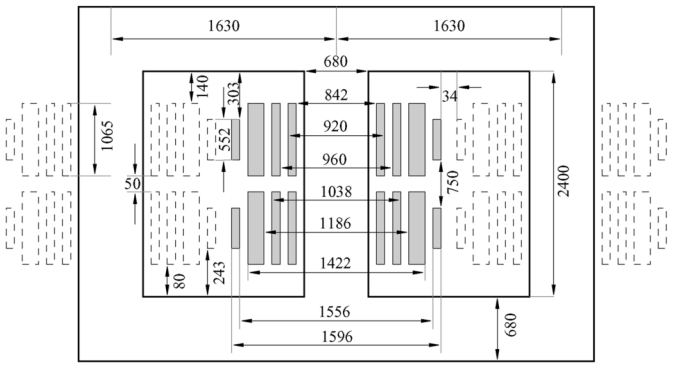

Fig. 10. Geometry details of analyzed split winding transformer (Courtesy: Crompton Greaves Ltd.).

TABLE X
B–H CURVE DATA

H (A/m)	10	15	20	25	30	50	100	200	300
B (T)	0.5	0.9	1.3	1.55	1.63	1.8	1.85	1.9	1.92

In the case of the postset method (with one winding short circuited), noticeable percentage of short-circuit current flows through the HV winding not facing directly the short circuited LV winding. This current is responsible for field distortion and increased axial forces.

Thus, the challenges posed while designing the split-winding transformers are exemplified in this work. The results obtained by such accurate coupled field-circuit analysis can be used to determine the electrical design parameters and the mechanical support structures for the windings.

APPENDIX
TRANSFORMER DESIGN AND NAMEPLATE DATA

Ratings of considered split-winding transformer: 70 MVA, three-phase, 220/6.9/6.9 kV, Y/Y/Y.

Nameplate and geometrical details are given in Table IX and Fig. 10, respectively. The material used for core is M3H and corresponding B–H curve data is given in Table X.

ACKNOWLEDGMENT

The authors would like to thank Crompton Greaves Ltd. for providing practical data on the split-winding transformer.

REFERENCES

[1] R. Tang, S. Wang, L. Yan, X. Wang, and C. Xiang, "Transient simulation of power transformers using 3–D finite element model coupled to electric circuit equations," *IEEE Trans. Magn.*, vol. 36, no. 4, pp. 1417–1420, May 2000.

[2] J.-S. Wang, "A nodal analysis approach for 2D and 3D magnetic-circuit coupled problems," *IEEE Trans. Magn.*, vol. 32, no. 3, pp. 1074–1077, May 1996.

[3] I. A. Tsukerman, A. Konrad, and J. D. Lavers, "A method for circuit connections in time-dependent eddy current problems," *IEEE Trans. Magn.*, vol. 28, no. 2, pp. 1299–1302, Mar. 1992.

[4] M. Waters, *The Short Circuit Strength of Power Transformers*. London, U.K.: Macdonald, 1966.

[5] K. Najdenkoski and D. Manov, "Electromagnetic forces calculation on power transformer winding under short circuit," *Int. J. Comput. Math. Elect. Electron. Eng.*, vol. 17, no. 1/2/3, pp. 374–377, 1998.

[6] C. M. Arturi, "Electromagnetic force calculation on a 3-phase autotransformer under time-varying fault by 3-D non-linear finite element code," *IEEE Trans. Magn.*, vol. 29, no. 2, pp. 2010–2013, Mar. 1993.

[7] C. M. Arturi, "3-D FE analysis of the axial forces on the step-up transformer winding with helical LV," *IEEE Trans. Magn.*, vol. 31, no. 3, pp. 2032–2035, May 1995.

[8] M. G. Kladas, M. P. Papadopoulos, and J. A. Tegopoulos, "Leakage flux and force calculation on power transformer windings under short circuit: 2D and 3D models on the theory of images and the finite element method compared to measurements," *IEEE Trans. Magn.*, vol. 30, no. 5, pp. 3487–3490, Sep. 1994.

[9] S. Salon, B. LaMattina, and K. Sivasubramaniam, "Comaparison of short ciruit forces in transformers," *IEEE Trans. Magn.*, vol. 36, no. 5, pp. 3521–3523, Sep. 2000.

[10] C. M. Arturi, "Electromagnetic force calculation on a 3-phase autotransformer under time-varying fault by 3-D non-linear finite element code," *IEEE Trans. Magn.*, vol. 29, no. 2, pp. 2010–2013, Mar. 1993.

[11] T. Renyan, L. Yan, L. Dake, and T. Lijian, "Numerical calculation of 3D transient eddy current field and short ciruit electromagnetic force in large transformers," *IEEE Trans. Magn.*, vol. 28, no. 2, pp. 1418–1421, Mar. 1992.

[12] S. L. Ho, Y. Li, H. C. Wong, S. H. Wang, and R. Y. Tang, "Numerical simulation of transient force and eddy current loss in a 720-MVA power transformer," *IEEE Trans. Magn.*, vol. 40, no. 2, pp. 687–690, Mar. 2004.

[13] P. Stuchl, I. Dolezel, A. Zajic, J. Hruza, and O. Weinberg, "Performance of transformer with split winding under nonstandard operation conditions," in *Proc. CIGRE*, 2000, pp. 12–103.

[14] G. Leber, "Investigation of inrush current during a short circuit test on a 440 MVA, 400 kV GSU-transformer," in *Proc. CIGRE*, 2000, pp. 12–104.

[15] S. V. Kulkarni and S. A. Khaparde, *Transformer Engineering: Design and Practice*. New York: Marcel Dekker, May 2004.

[16] M. Steurer and K. Frohlich, "The impact of inrush current on the mechanical stress of high voltage power transformer coils," *IEEE Trans. Power Del.*, vol. 17, no. 1, pp. 155–160, Mar. 1993.

[17] J. Jin, *The Finite Element Method in Electromagnetics*. New York: Wiley, 2000.

[18] M. V. K. Chari and S. J. Salon, *Numerical Methods in Electromagnetism*. London, U.K.: Academic, 2000.

G. B. Kumbhar received the B.E. degree in electrical engineering from the Government College of Engineering, Maharashtra, India, in 1999 and the M.Tech. degree from the Indian Institute of Technology–Madras, Chennai, in 2002.

He is presently a Research Scholar at the Indian Institute of Technology-Bombay, Mumbai, working in the area of coupled field formulations in transformers.

S. V. Kulkarni (M'99) is Associate Professor, Department of Electrical Engineering, Indian Institute of Technology, Bombay, India. Previously, he worked at Crompton Greaves Ltd., and specialized in the design and development of transformers up to the 400-kV class. He authored the book *Transformer Engineering: Design and Practice* (New York: Marcel Dekker). His research interests include transformer design and analysis, computational electromagnetics, and distributed generation.

Mr. Kulkarni is the recipient of the Young Engineer Award (2000) from the Indian National Academy of Engineering.